DOI: https://dx.doi.org/10.4314/gjpas.v32i5.8

GLOBAL JOURNAL OF PURE AND APPLIED SCIENCES VOL. 32, 2026: 767-781
 ISSN 1118 – 0579, e-ISSN: 2992 - 4464
www.globaljournalseries.com.ng, Email: globaljournalseries@gmail.com

TRANSIENT MHD NANOFLUID CONVECTION WITH COUPLED HEAT–MASS TRANSFER OVER AN INCLINED POROUS MEDIUM FOR THERMAL REGULATION AND MATERIAL ENGINEERING

ARONY LUCAS AND THOMAS I. CHUWA
Corresponding author's E-mail: ronnylucas1002@gmail.com

(Received 28 April 2026; Revision Accepted 20 June 2026)

ABSTRACT

This study explores the unsteady MHD flow of a reactive, radiative, heat-generating nanofluid past an infinite inclined porous plate, influenced by mixed convection and coupled thermal-solutal diffusion (Soret and Dufour effects). The nanofluid consists of water-based Cu-Ag nanoparticles. The governing non-dimensional quasi-linear PDEs are formulated with appropriate initial and boundary conditions and solved numerically using an explicit finite difference method implemented in Fortran. The impact of various flow parameters on velocity, temperature, and concentration profiles is examined through graphs, while skin friction, heat transfer (Nusselt number), and mass transfer (Sherwood number) rates are presented in tables. Results show that permeability, heat source, Dufour number, and buoyancy enhance fluid motion and mass transport, whereas magnetic field strength, chemical reaction rate, and inclination angle reduce velocity. Thermo-diffusion raises fluid temperature, while higher chemical reaction and Schmidt numbers lower concentration. A comparison with existing studies demonstrates strong agreement, confirming the model's reliability.

KEYWORDS: Magnetohydrodynamics (MHD), Nanofluid Convection, Heat and Mass Transfer, Soret Effect (Thermo-diffusion), Dufour Effect (Diffusion-thermo), Porous Medium, FDM, Inclination Angle, Heat Generation

INTRODUCTION

Growing awareness of global energy sustainability challenges has led to increased interest in enhancing energy efficiency, particularly in heat transfer applications. Various strategies have been adopted to improve convective heat transfer performance, including modifications to flow geometry, boundary conditions, and enhancement of thermal conductivity. It is well established that metals exhibit significantly higher thermal conductivities than conventional fluids. By dispersing metallic nanoparticles into base fluids, thermal conductivity can be effectively improved—resulting in the formation of nanofluids. This concept was first introduced by Choi [1], whose pioneering work demonstrated notable improvements in heat transfer performance. Building on Choi's findings, numerous studies have investigated the thermal behavior of nanofluids and their potential in advanced thermal systems [2–9].

The study of thermal and solutal transport involving reacting species holds substantial practical importance for engineers and scientists, owing to its widespread presence across various scientific and technological fields. Such flows are particularly relevant in industries such as power generation and chemical processing. Balla et al. [10] investigated the impact of chemical reactions on bio-convective flow involving oxytactic microorganisms within a permeable medium. Shamshuddin et al. [11] analyzed the heat and mass transfer performance of Cu/CuO nanoparticles over a radiating stretching sheet, considering heat generation/absorption and chemical reactions. Puneeth et al. [12] examined bioconvective flow of a radiating hybrid nanofluid past a steel blade under the influence of heterogeneous and homogeneous chemical reactions. Additionally, several studies [13–17] have explored the effects of chemical reactions on MHD nanofluid transport, incorporating various flow parameters and geometries.

Arony Lucas, Department of Applied Science and Social Studies, Arusha Technical College, P.O. Box 296, Arusha, Tanzania
Thomas I. Chuwa, Department of Transportation Engineering, Arusha Technical College, P.O. Box 296, Arusha, Tanzania

Thermal radiation effects have garnered significant attention from researchers due to their wide-ranging applications in science and engineering, including medical therapies, food preservation, solar energy systems, and electrical technologies. Roja and Gireesha [18] analyzed the impact of Hall and ion effects on radiative, heat-generating, hydro-magnetic nanofluid flow through an inclined channel under convective and velocity slip conditions. Kumar et al. [19] investigated the influence of thermal radiation on natural convective MHD nanofluid flow over a suddenly accelerated vertical plate. Reddy et al. [20] examined heat transfer characteristics in MHD radiative, viscous dissipative, and chemically reactive Casson nanofluid flow over a nonlinear stretching surface. Several studies [21–24] have also highlighted the role of radiative energy interactions in MHD nanofluid transport under various flow configurations. Gopal et al. [25] reported the transient behavior of radiative MHD free convection nanofluid flow past an infinite vertical porous plate.

The effects of thermal-diffusion (Soret effect) on hydromagnetic boundary layer flow have attracted considerable attention due to their critical role in advanced technological designs and high-efficiency industrial processes. Soret effects have notable applications in geophysics, oceanography, and chemical engineering processes such as isotope separation in gas mixtures involving light (H_2, He) and medium (N_2, air) molecular weight gases. Recognizing these practical applications, Singha et al. [26] examined the influence of thermo-diffusion and diffusion-thermo (Dufour effect) on MHD flow of water-based nanofluids over an exponentially stretching surface embedded in a non-Darcian porous medium. Padmaja and Kumar [27] studied the impact of Soret and Dufour effects on MHD transport of Cu-water and Al_2O_3-water nanofluid flows past a permeable rotating cone. Siddique et al. [28] explored the role of these effects in the transient MHD flow of a second-grade nanofluid across an exponentially expanding sheet. Additional studies [29–30] have further addressed diffusive transport effects in MHD nanofluid systems.

A critical review of the existing literature reveals several gaps that motivate the present study. First, most studies on MHD nanofluid flow over inclined porous plates consider either Soret or Dufour effects in isolation, but rarely incorporate both simultaneously alongside thermal radiation, chemical reaction, and heat generation in a transient framework [26–30]. Second, while hybrid nanofluids comprising two distinct nanoparticle species (such as Cu and Ag) offer superior thermophysical properties compared to mono-nanofluids, their combined double-diffusive behavior over inclined geometries under a magnetic field remains insufficiently explored. Third, studies that do consider inclined plates with MHD effects, such as Haritha et al. [29] and Raghunath [30], restrict their attention to single-species nanofluids and do not account for the Dufour effect. Similarly, Siddique et al. [28] examined Soret and Dufour effects in transient MHD flow but used a second-grade non-Newtonian fluid over an exponentially stretching sheet, a configuration that differs markedly from the inclined porous plate geometry examined here. The present study therefore addresses these combined gaps by integrating all of these physical effects within a unified transient model. The novelty of the present work lies in the simultaneous consideration of the following features, which, to the best of the authors' knowledge, have not been collectively addressed in any prior study: (i) transient (unsteady) MHD free convection of a Cu-Ag water-based hybrid nanofluid past an infinite inclined porous plate; (ii) coupled Soret (thermo-diffusion) and Dufour (diffusion-thermo) effects acting together with thermal radiation and internal heat generation; (iii) first-order chemical reaction influencing species concentration; and (iv) mixed (thermal and solutal) buoyancy driving the flow simultaneously. Unlike Gopal et al. [25], who considered a vertical plate without Soret/Dufour effects, and unlike Singha et al. [26], who used an exponentially stretching non-Darcian geometry, the present configuration of an inclined plate with all the above physics represents a closer approximation to real industrial systems such as inclined solar collectors, chemical reactors with slanted walls, and oblique-flow pharmaceutical drying equipment. The governing dimensionless PDEs are solved using an explicit finite difference method (FDM) implemented in Fortran, and results are validated against the benchmark data of Gopal et al. [25], confirming the reliability of the numerical procedure.

Considering the practical applications, the above literature cited, the object of this current work is to examine the double-diffusive effects on time-dependent magnetohydrodynamic (MHD) free convective nanofluid transport past an inclined vertical porous plate. This model problem will have critical applications in chemical industries such as food processing, catalytic chemical reactors, polymer production, manufacturing of ceramics or glassware, food preservation, polymer manufacture, purification of crude oil, isotope separation, as manufacturing of pharmaceutical products etc. The modeled dimensionless governing flow of partial differential equations have been solved numerically using an explicit FDM. The precision of the computed numerical structure was achieved by comparing the present results with previously published solutions, and excellent agreement was found.

2. Model description

Consider the time-dependent MHD natural convective transport of a nanofluid past an infinite inclined vertical porous plate set into impulsive motion. Firstly, the plate is at zero velocity with the ambient temperature θ'_∞.

At time $t > 0$, the plate begins to change position in its plane with the velocity $U_0\tau^*$ in the skyward direction, where U_0 is consistent, and the temperature of the plate is elevated or dropped to θ'_w. We select the $x'-$axis along the plate in the upward inclined direction and $z'-$axis perpendicular to the plate. A uniform transverse magnetic field of strength B_0 is employed parallel to the $z'-$axis. The plate matches the plane $z' = 0$ and the flow being restricted to $z' > 0$. The physical model of the flow is illustrated in Figure 1. The assumptions of the present problem are made as follows. The pressure gradient is neglected in this problem. A radiative heat flux q_r is introduced in the normal direction to the plate. The fluid is a water-based nanofluid comprising two types of nanoparticles Cu and Ag. It is assumed that the induced magnetic field produced by the fluid motion is negligible in comparison with the applied one, so that we consider the magnetic field $B = (0,0,B_0)$. This assumption is justified, since the magnetic Reynolds number is very small for metallic liquids and partially ionized fluids. Under the above assumptions, the momentum, energy equations, and concentration equations can be expressed as:

$$\rho_{nf}\frac{\partial v'}{\partial \tau'} = \mu_{nf}\frac{\partial^2 v'}{\partial z'^2} - \sigma_{nf}B_0{}^2 v' + \frac{\mu_{nf}\phi^*}{k}v' + g(\rho B_1)_{nf}(\theta' - \theta_\infty{}')(\cos\alpha) + g(\rho\beta_2)_{nf}(\phi' - \phi'_\infty)(\cos\alpha) \quad (1)$$

$$\frac{\partial \theta'}{\partial \tau'} = \frac{k_{nf}}{(\rho c_p)_{nf}}\frac{\partial^2 \theta'}{\partial z'^2} - \frac{1}{(\rho c_p)_{nf}}\frac{\partial q_r}{\partial z'} + \frac{D_m k_T}{c_s c_p}\frac{\partial^2 \phi'}{\partial z'^2} + \frac{1}{(\rho c_p)_{nf}}Q^*(\theta' - \theta_\infty{}') \quad (2)$$

$$\frac{\partial \phi'}{\partial \tau'} = D_{nf}\frac{\partial^2 \phi'}{\partial z'^2} - k'_r(\phi' - \phi'_\infty) + \frac{D_m k_T}{T_m}\frac{\partial^2 \phi'}{\partial z'^2} \quad (3)$$

Where $v', \theta', \phi', \rho_{nf}, \mu_{nf}, \sigma_{nf}, (\rho B_1)_{nf}, (\rho\beta_2)_{nf}, g, \phi^*, Q^*, (\rho C_p)_{nf}, k_{nf}, D_{nf}, k'_r, D_m, T_m, k_T, \alpha$ is fluid velocity, nanofluid temperature, nanofluid concentration, nanofluid density, dynamic viscosity of nanofluid, electrical conductivity of nanofluids, thermal expansion coefficient, coefficient of volumetric expansion, acceleration due to gravity, porosity of the porous medium, heat absorption constant, specific heat capacity of the nanofluid, thermal conductivity of nanofluid, mass diffusivity, chemical reaction parameter, chemical molecular diffusivity, thermal diffusion rate, and inclination angle respectively. And the characteristic time t_0 is defined as $\tau_0 = \frac{v_f}{U_0^2}$

For nanofluids, the parameters $\rho_{nf}, \mu_{nf}, (\rho c_p)_{nf}, (\rho B_T)_{nf}, (\rho\beta_c)_{nf}, \sigma_{nf}$ are demarcated as:

$$\rho_{nf} = (1-\phi)\rho_f + \phi\rho_s, \quad \mu_{nf} = \frac{\mu_f}{(1-\phi)^{2.5}}, \quad (\rho c_p)_{nf} = (1-\phi)(\rho c_p)_f + \phi(\rho c_p)_s,$$

$$(\rho B_T)_{nf} = (1-\phi)(\rho B_T)_f + \phi(\rho B_T)_s, \quad \sigma_{nf} = \sigma_f\left(1 + \frac{3(\sigma-1)\phi}{(\sigma+2)-(\sigma-1)\phi}\right) \text{ where } \sigma = \frac{\sigma_f}{\sigma_s},$$

$$\frac{k_{nf}}{k_f} = \frac{k_s + 2k_f - 2\phi(k_f - k_s)}{k_s + 2k_f + \phi(k_f - k_s)},$$

Where $\phi, \rho_f, \rho_s, \sigma_f, \sigma_s, \mu_f, (\rho c_p)_f, (\rho c_p)_s, k_f, k_s$ is the nanoparticle volume fraction, density of the base fluid, density of the nanoparticles, electrical conductivity of the base fluid, electrical conductivity of the nanoparticles, viscosity of the base fluid, heat capacitance of the base fluid, heat capacitance of the nanoparticles, thermal conductivity of the base fluid, and thermal conductivity of the nanoparticles respectively.

The appropriate initial and boundary conditions for the flow are:

$$\left.\begin{array}{lll} v'=0,\ \ \theta'=\theta'_\infty,\ \phi'=\phi'_\infty & \text{for all } z' \quad \text{and} & \tau'\le 0 \\ u'=U_0\tau^*,\ \ \theta'=\theta'_w,\ \phi'=\phi'_w & \text{at}\ \ z'=0 \quad \text{for} & \tau'>0 \\ u'\to 0,\ w'\to 0,\ \theta'\to\theta'_w,\ \phi'=\phi'_w & \text{as}\ \ z'\to\infty \ \ \text{for} & \tau'>0 \end{array}\right\} \tag{4}$$

$v',\theta',\phi',\rho_{nf},\mu_{nf},\sigma_{nf},(\rho B_1)_{nf},(\rho\beta_2)_{nf},g,\psi,Q^*,(\rho C_p)_{nf},k_{nf},D_{nf},k'_r,D_m,T_m,k_T$ All symbols are as defined above following Eq. (3). t_0 is defined as $\tau_0=\dfrac{v_f}{U_0^2}$

For nanofluids, the expressions of $\rho_{nf},\mu_{nf},(\rho c_p)_{nf},(\rho B_T)_{nf},(\rho\beta_c)_{nf},\sigma_{nf}$ are defined as:

$$\rho_{nf}=(1-\phi)\rho_f+\phi\rho_s,\ \ \mu_{nf}=\frac{\mu_f}{(1-\phi)^{2.5}},\ \ (\rho c_p)_{nf}=(1-\phi)(\rho c_p)_f+\phi(\rho c_p)_s,$$

$$(\rho B_T)_{nf}=(1-\phi)(\rho B_T)_f+\phi(\rho B_1)_s,\ \ \sigma_{nf}=\sigma_f\left(1+\frac{3(\sigma-1)\phi}{(\sigma+2)-(\sigma-1)\phi}\right)\ \ \text{where } \sigma=\frac{\sigma_f}{\sigma_s}\ ,$$

$$\frac{k_{nf}}{k_f}=\frac{k_s+2k_f-2\phi(k_f-k_s)}{k_s+2k_f+\phi(k_f-k_s)},$$

Where $\phi,\rho_f,\rho_s,\sigma_f,\sigma_s,\mu_f,(\rho c_p)_f,(\rho c_p)_s,k_f,k_s$ is the nanoparticle volume fraction, density of the base fluid, density of the nanoparticles, electrical conductivity of the base fluid, electrical conductivity of the nanoparticles, viscosity of the base fluid, heat capacitance of the base fluid, heat capacitance of the nanoparticles, thermal conductivity of the base fluid, and thermal conductivity of the nanoparticles respectively.

The Rosseland approximation applies to optically thick media and gives the net radiation heat flux q_r through the expression as,

$$q_r=-\frac{4\sigma'}{3k'}\frac{\partial\theta'^4}{\partial z'} \tag{5}$$

where σ' and k' denote respectively, the Stefan-Boltzmann constant and absorption coefficient. It is supposed that the temperature difference $\theta'-\theta_\infty{}'$ within the boundary layer flow is sufficiently small such that the term θ'^4 may be expressed as a linear function of temperature. This is done by expanding θ'^4 in a Taylor series about a free stream temperature $\theta_\infty{}'$ as pursues

$$\theta'^4=\theta'^4_\infty+3\theta'^3_\infty(\theta'-\theta'_\infty)+6\theta'^2_\infty(\theta'-\theta'_\infty)^2+\ldots \tag{6}$$

Neglecting higher order terms in Eq. (6) ahead of the first order in $(\theta'-\theta'_\infty)$, we attain,

$$\theta'^4\cong 4\theta'^3_\infty\theta'-3\theta'^4_\infty \tag{7}$$

Differentiating equation (7) with respect to z' we obtain

$$\frac{\partial\theta'^4}{\partial z'}=4\theta'^3_\infty\frac{\partial\theta'}{\partial z'} \tag{8}$$

Now substitute equation (8) into equation (5)

$$q_r=-\frac{4\sigma'}{3k'}\left(4\theta'^3_\infty\frac{\partial\theta'}{\partial z'}\right)=-\frac{16\sigma'\theta'^3_\infty}{3k'}\frac{\partial\theta'}{\partial z'} \tag{9}$$

Differentiating q_r with respect to z' one acquires

$$\frac{\partial q_r}{\partial z'}=-\frac{16\sigma'\theta'^3_\infty}{3k'}\frac{\partial^2\theta'}{\partial z'^2} \tag{10}$$

Substituting equation (10) in equation (2) results

$$\frac{\partial\theta'}{\partial\tau'}=\frac{k_{nf}}{(\rho c_p)_{nf}}\frac{\partial^2\theta'}{\partial z'^2}-\frac{1}{(\rho c_p)_{nf}}\left(k_{nf}+\frac{16\sigma'\theta_\infty'^3}{3k'}\right)\frac{\partial^2\theta'}{\partial z'^2}-\frac{1}{(\rho c_p)_{nf}}Q^*(\theta'-\theta_\infty{}')+\frac{D_m k_T}{c_s c_p}\frac{\partial^2\phi'}{\partial z'^2} \tag{11}$$

Introducing dimensionless parameters

$$\left.\begin{aligned}
&v=\frac{v'}{U_0},z=\frac{U_0 z'}{v_f},\tau=\frac{U_0^2\tau'}{v_f},\theta=\frac{\theta'-\theta_\infty'}{\theta_w'-\theta_\infty{}'},C=\frac{\phi'-\phi_\infty'}{\phi_w'-\phi_\infty'},M^2=\frac{\beta_3 v_f\sigma_f B_0^2}{\rho_{nf}U_0^2},R=\frac{16\sigma_1 T_\infty'^3}{3kk^*},\\
&K_1=\frac{kU_0^2}{v_{nf}\phi^* v_f},P_r=\frac{(\mu c_p)_f}{k_f},G_r=\frac{v_f g\beta_{1Tf}(\theta_w'-\theta_\infty{}')}{U_0^3},G_m=\frac{v_f g\beta_{2f}(\phi_w'-\phi_\infty')}{U_0^3},S_c=\frac{v_f}{D_{nf}},\\
&Q_s=\frac{v_f Q^*(\phi_w'-\phi_\infty')}{U_0^2(\theta_w'-\theta_\infty{}')}\gamma=\frac{k_r' v_f}{U_0{}^2},S_r=\frac{D_m k_T(\theta_w'-\theta_\infty{}')}{v_f T_m(\phi_w'-\phi_\infty')},D_u=\frac{D_m k_T}{vc_s c_p}\frac{(\phi_w'-\phi_\infty')}{(\theta_w'-\theta_\infty{}')},
\end{aligned}\right\} \tag{12}$$

Utilizing of dimensionless variables, the governing Eqs. (1), (3) and (11) reduces to

$$\frac{\partial v}{\partial\tau}=\frac{1}{R_e}\frac{\partial^2 v}{\partial z^2}-M^2 v-\frac{1}{K_1}v+y_1 G_T T(\cos\alpha)+y_2 G_C C(\cos\alpha), \tag{13}$$

$$\frac{\partial T}{\partial\tau}=\frac{1}{b_1}\left(\frac{1+R}{P_r}\right)\frac{\partial^2 T}{\partial z^2}+Q_1 T+D_u\frac{\partial^2 C}{\partial z^2}, \tag{14}$$

$$\frac{\partial C}{\partial\tau}=\frac{1}{S_c}\left(\frac{\partial^2 C}{\partial z^2}\right)+S_r\left(\frac{\partial^2 T}{\partial z^2}\right)-\gamma C \tag{15}$$

Where $R_e, M^2, P_r, G_T, G_C, S_c, K_1, R, Q_1, S_r, D_u$ Reynolds number, Magnetic field parameter, Prandtl number, thermal Grashof number, solutal Grashof number, Schmidt number, porosity parameter, thermal radiation parameter, dimensionless heat source parameter, Soret number, and Dufour number respectively.
Parameters and variables appearing in Eq (12-15) are defined as:

$$R_e=(1-\phi)^{2.5}\left[(1-\phi)+\phi\left(\frac{\rho_s}{\rho_f}\right)\right],\quad b_1=\frac{\beta_4}{\lambda_{nf}},\quad \lambda_{nf}=\frac{k_{nf}}{k_f},$$

$$y_1=\frac{(1-\phi)\rho_f-\phi\rho_s\left(\dfrac{\beta_{1s}}{\beta_{1f}}\right)}{\rho_{nf}},\quad y_2=\frac{(1-\phi)\rho_f-\phi\rho_s\left(\dfrac{\beta_{2s}}{\beta_{2f}}\right)}{\rho_{nf}}$$

$$\beta_3=1+\frac{3(\sigma-1)\phi}{(\sigma+2)-(\sigma-1)\phi},\quad \beta_4=(1-\phi)+\phi\left(\frac{(\rho c_p)_s}{(\rho c_p)_f}\right)$$

The initial and boundary conditions in dimensionless form are specified as:

$$\left.\begin{array}{llll}
\tau\le 0; & v=0, & T=0,\ C=0, & \text{for all } z\\
\tau>0; & v=\tau^*, & T=1,\ C=1, & \text{at } z=0\\
v\to 0; & T\to 0, & C\to 0, & \text{as } z\to\infty
\end{array}\right\} \tag{16}$$

The thermal-physical properties of base fluid and nanoparticles are portrayed in table 1 as follows:

Table 1: Thermal-physical properties of nanofluids

	H_2O	Ag	Cu
$c_p(kg^{-1}K^{-1})$	4179	235	385
$\rho(kgm^{-3})$	997.1	1.05×10^4	8933
$k(Wm^{-1}K^{-1})$	0.613	429	401
$\beta\times10^{-5}(K^{-1})$	21	1.89	1.67
$\sigma(S/m)$	5.5×10^{-6}	62.1×10^6	$5.9.6\times10^6$

With considerable physical engineering properties analogous to thermal and solutal flow potentials encompass the wall-friction coefficient τ_x, heat and mass transfer rates in terms of Nusselt number N_u, and Sherwood number S_h, which are described in dimensionless form by

$$C_f = \left(\frac{\partial v}{\partial z}\right)_{z=0}, N_u = \left(\frac{\partial T}{\partial z}\right)_{z=0} \text{ and } S_h = \left(\frac{\partial C}{\partial z}\right)_{z=0}.. \quad (17)$$

3. Computation Scheme

The coupled quasi-linear PDEs $(13)-(15)$ collectively with initial and boundary regulations Eq. (16) represents the flow determining equations of the proposed model. The analytical (exact) solutions to mentioned equations are practically almost not possible. Thus, the explicit finite difference scheme is prescribed to solve Eqs. $(13)-(15)$ along with Eqs. (16). The following are steps used in the solution;

i. Define the Problem
ii. Discretize the Domain
iii. Approximate the Derivatives
iv. Rearrange the equation
v. Apply the initial and boundary conditions
vi. Compute the First Time Step
vii. Perform Time-Stepping

Subjected to the transformed initial and boundary conditions:

$$\left.\begin{array}{ll} \tau\le 0; \quad v_{i,j}=0, \quad T_{i,j}=0,\ C_{i,j}=0, & \text{for all } i \text{ and } j \\ \tau>0; \quad v_{i,j}=\tau^*, \quad T_{i,j}=1,\ C_{i,j}=1, & \text{at } i=0 \quad \text{for } j>0 \\ v_{i,j}\to 0;\ T_{i,j}\to 0, \quad C_{i,j}\to 0, & \text{as } i\to\infty \ \text{ for } j>0 \end{array}\right\} \quad (21)$$

Here, index i characterizes the space $y,\Delta z$ signify mesh in $y-$ direction; index j characterizes the temporal τ, and $\Delta\tau$ represents the mesh in $\tau-$ direction. Thus, the values of flow variables such as $u,\ C,$ and T at grid point $\tau=0$ are identified; hence the velocity field, concentration field and thermal field has been solved at time $\tau_{j+1}=\tau_j+\Delta\tau$ using the known values of the previous time $\tau=\tau_j$ for all $j=0,1,2,...N-1$. These processes are repeated till the required solution of velocity field, concentration field, and temperature field converge. The mesh size is fixed at $\Delta\tau=0.0125$ and $\Delta z=0.025$ for the whole computational process to ensure stability and convergence of the numerical solution.

Stability analysis

The Courant governs the stability and convergence of the explicit finite difference scheme–Friedrichs-Lewy (CFL) condition. For the momentum equation, the stability requirement imposes that the time step Δt and spatial step Δy satisfy the condition $\Delta t \le (\Delta y)^2 / (2v)$, where v denotes the kinematic viscosity of the nanofluid. Similarly, for the energy and concentration equations, the respective diffusion-stability constraints require $\Delta t \le (\Delta y)^2 / (2\alpha)$ and $\Delta t \le (\Delta y)^2 / (2D)$, where α is the thermal diffusivity and D is the mass diffusivity of the nanofluid. With the selected mesh parameters $\Delta y = 0.05$ and $\Delta t = 0.005$, all three stability conditions are satisfied for the range of Prandtl and Schmidt numbers considered in this study (Pr = 6.2 for water and Sc = 0.60–3.00).

The convergence of the iterative solution was verified by monitoring the maximum absolute change in velocity, temperature, and concentration between successive time steps. Computations were terminated and steady-state was declared when this change fell below a prescribed tolerance of 10^{-5} for all three fields simultaneously. Grid independence was also confirmed by comparing results at $\Delta y = 0.05$ with those at $\Delta y = 0.025$; the maximum deviation in the Nusselt number was found to be less than 0.01%, confirming that the selected mesh is sufficiently refined.

The parameter values used in the numerical simulations are chosen to reflect physically realistic scenarios consistent with prior literature. The Prandtl number Pr = 6.2 corresponds to water at approximately 25°C, which is the standard base fluid for Cu–Ag nanofluids at moderate temperatures. The magnetic parameter M is varied in the range 1–5, representing moderate applied magnetic fields typical of laboratory-scale MHD experiments and industrial cooling channels where electromagnetic braking is employed to regulate flow. The Schmidt number Sc is varied from 0.60 to 3.00, covering diffusing species ranging from hydrogen (Sc ≈ 0.22) to heavier hydrocarbons and pharmaceutical solutes (Sc > 2), making the results applicable to isotope separation, drug manufacturing, and polymer processing. The heat-generation parameter Q_1 takes positive values (0.5–2.0), representing internal heat sources such as exothermic chemical reactions or Joule heating, while the chemical-reaction parameter Kr is varied from 1 to 3, corresponding to weak-to-moderate first-order destructive reactions common in catalytic reactor systems. The inclination angle α is varied from 15° to 75° to simulate a range of industrial surfaces from near-horizontal dryers to near-vertical reactor walls. The Soret (Sr) and Dufour (Du) numbers are selected such that their product Sr × Du remains constant (approximately 0.4) in accordance with the Onsager reciprocal relation, a constraint widely adopted in cross-diffusion studies [26–28]. These selections collectively ensure that the parametric study is physically grounded and directly interpretable in the context of the industrial applications cited.

4. Verification of the numerical scheme

To validate the numerical procedure, the present Nusselt number results are compared with those of Gopal et al. [25] in Table 2. Excellent agreement is observed across all parameter variations, confirming the accuracy of the developed Fortran code.

Table 2: Comparison of Nusselt number when $G_C = 0, S_r = 0, D_u = 0$ and $\gamma = 0$

M	K_1	R	ϕ	Gopal et al. [25]	Present work
2.00	0.50	1.00	0.05	0.522145	0.522149
3.00	-	-	-	0.458496	0.458486
4.00	-	-	-	0.355447	0.355456
-	1.00	-	-	0.565852	0.565843
-	1.50	-	-	0.605241	0.605251
-	-	1.50	-	0.587463	0.587460
-	-	2.00	-	0.622447	0.622435
-	-	-	0.20	0.597996	0.597991
-	-	-	0.40	0.650621	0.650624

RESULTS AND DISCUSSION

To inspect the physical worth of the modeled problem, the influence of various pertinent parameters fused in the problem such as magnetic parameter M, heat generation parameter Q_1, radiation parameter R, Soret number S_r, chemical reaction parameter γ, Prandtl number P_r, Schmidt number S_c, Dufour parameter D_u, absorbent parameter K_1, inclination angle α, thermal Grashof number G_T and mass Grashof number G_C on the nanofluid momentum, temperature and concentration are presented graphically. Shear stress, Nusselt number and Sherwood number are calculated numerically and presented in tabular format. The numerical calculations have been done by considering the constant values of several involved parameters in the problem as $P_r = 0.71,\ R = 1,\ Q = 1,\ D_u = 0.1,\ \gamma = 1,\ S_c = 0.6,\ R_e = 0.7,\ G_T = 1,\ G_C = 0.01,\ M = 2,\ K_1 = 1.0,\ \alpha = \pi/6,$ and $S_r = 0.1,$ until otherwise stated

MOMENTUM PROFILES

Fig. 2 illustrates the impact of Prandtl number P_r on nanofluid velocity. It is clearly observed that fluid velocity decreases with rise in Prandtl number.

Virtually, an escalation in P_r tends to increase fluid viscosity; consequently, the fluid becomes thicker, kinetic energy is suppressed, and fluid temperature decreases. Fig. 3 exhibits the effect of radiation R on fluid velocity. It is observed that increasing values of R enhance the magnitude of the thermal and momentum boundary layers which gives an increasing effect on fluid motion. Figure 4 displays the impact of chemical reaction parameter γ on the velocity profiles. It is clearly observed that an increase in the chemical reaction parameter causes a decline in fluid velocity. The impact of heat-generating parameter Q_1 on fluid velocity is shown in Fig. 5. It is observed that increasing values of Q_1 result in enhancement of fluid momentum. Practically, when heat is generated to the fluid, kinetic energy is raised within the flow regime hence momentum of the fluid increases. Fig. 6 shows the variation of fluid velocity for different values of the magnetic parameter M. Increasing the magnetic parameter M, causes the fluid velocity in the boundary layer to diminish due to the Lorentz force, which acts in the reverse direction of the fluid flow, subsequently reducing the fluid velocity. The variation of the velocity distribution is depicted in fig. 7 for various values of S_c. A retarding effect on the fluid velocity is observed with increasing values of S_c due to the heavier diffusing species. We remarked from Figs. 8 and 9, that for heightening values of thermal and mass Grashof parameters G_T and G_C, the fluid momentum increases within the boundary layer. This is because the thermal Grashof number G_T stipulate the buoyancy strength to viscid force ratio. For evolving G_T values, buoyancy forces dominate the flow and accelerate the fluid momentum. Similarly, increasing values of the mass Grashof number G_C mounting G_C values progressively strengthen the solutal buoyancy force, resulting in enhanced fluid velocity. Fig. 10 shows the effect of the permeability parameter K_1 on the profiles of velocity. It is marked that, for bigger values of K_1, reduce the thickness of the velocity boundary layer. Physically, a higher permeability parameter reduces resistance to flow within the porous medium adjacent to the surface, ultimately accelerating the fluid velocity. The effects of the Dufour parameter on velocity profile is portrayed in fig. 11. It is observed that growing values of the Dufour number enhance fluid velocity throughout the boundary layer. Physically, the Dufour effect generates heat energy through concentration gradients, increasing the kinetic energy of fluid molecules and thereby boosting fluid momentum. The variation of fluid velocity with inclination angle α is shown in Fig. 12. It is observed that larger inclination angles α tends to lessen the fluid velocity. The alteration of the velocity dprofile with the time factor τ is shown in Fig. 13. From this figure, it is observed that fluid velocity increases progressively with time.

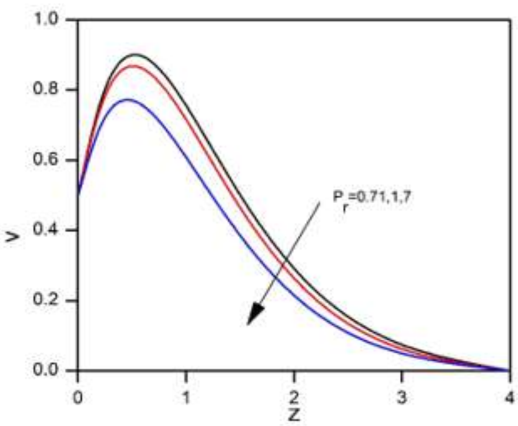

Fig 2: Momentum profile v with P_r values

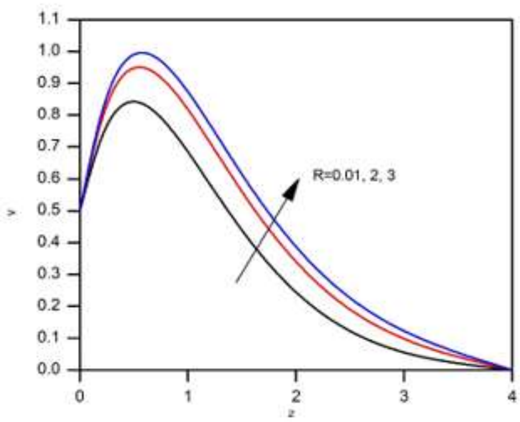

Fig 3: Momentum profile v with R values

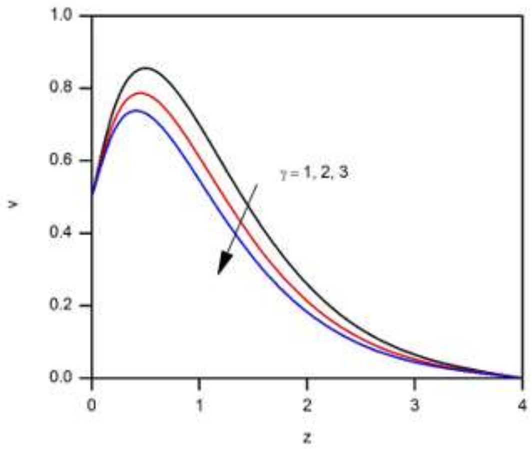

Fig 4: Momentum profile v with γ values

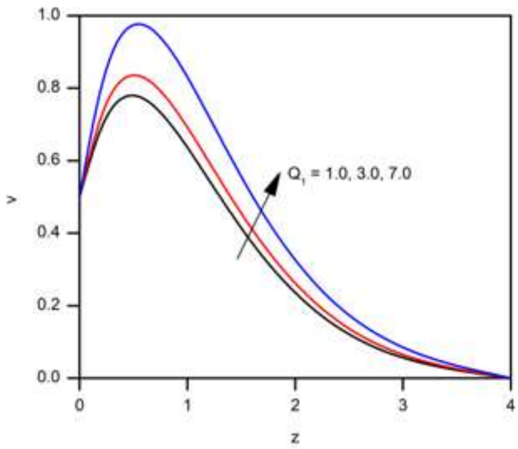

Fig 5: Momentum profile v with Q_1 values

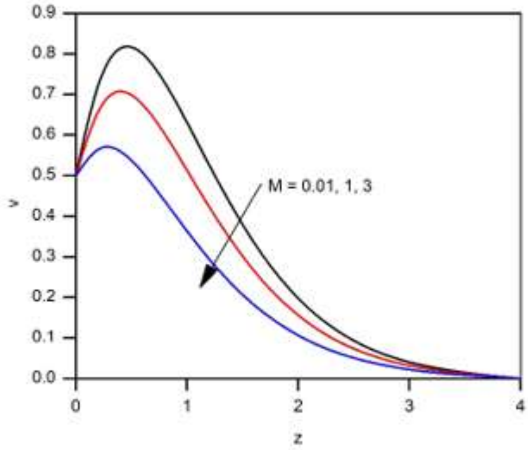

Fig 6: Momentum profile v with M values

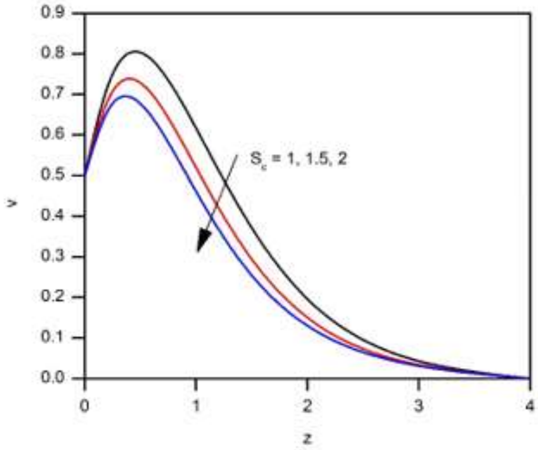

Fig 7: Momentum profile v with S_c values

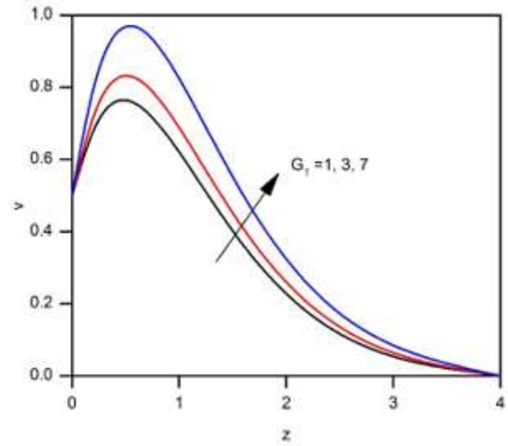

Fig 8: Momentum profile v with G_T values

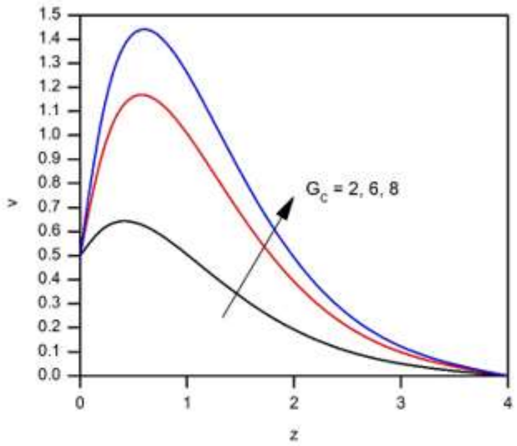

Fig 9: Momentum profile v with G_C values

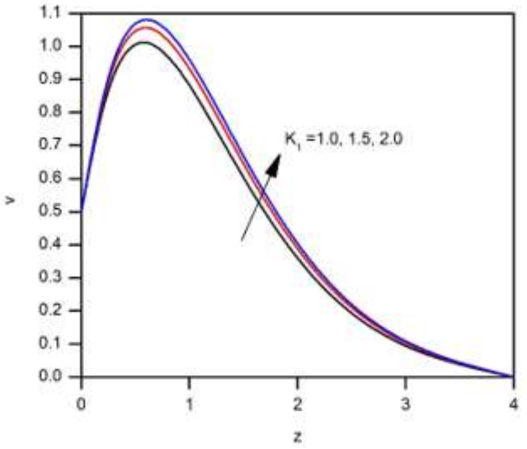

Fig 10: Momentum profile v with K_1 values

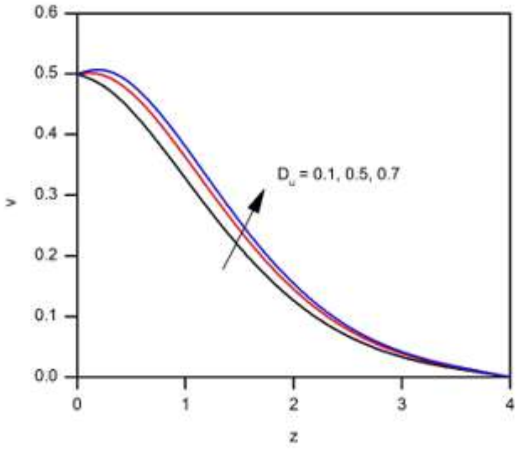

Fig 11: Momentum profile v with D_u values

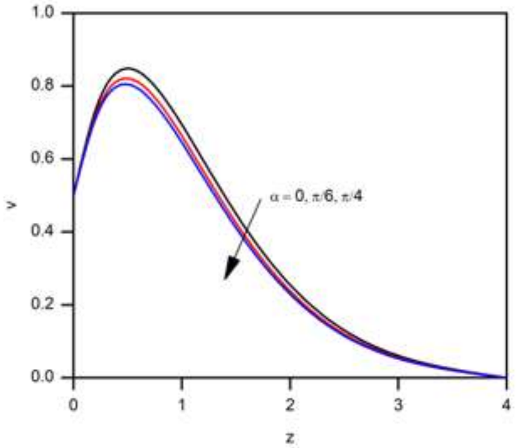

Fig 12: Momentum profile v with α values

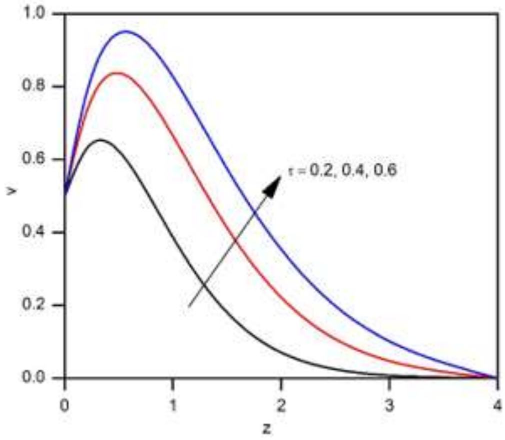

Fig 13: Momentum profile v with τ values

Temperature profiles

Fig.14 displays the influence of heat-generating parameter Q_1 on fluid temperature. It is observed that increasing values of Q_1 marks to enhancement of fluid temperature. Essentially, when heat is produced to the fluid, kinetic energy is raised within the fluid field hence temperature of the fluid is raised. Fig. 15 explains the effect of Prandtl number P_r on fluid temperature. It is observed that fluid temperature decreases with higher values P_r. The cause behind this is, higher values of P_r implies that thermal diffusivity is relatively small compared to momentum diffusivity, meaning that heat diffuses more slowly through the fluid. Consequently, for fluids with high P_r heat propagation within the fluid takes a long time, leading slower rate of temperature change. The effect of thermal radiation R is illustrated in Fig. 16. It is detected that temperature of the fluid raises with higher value of R. Physically, when the fluid is subjected to thermal radiation, it absorbs radiant energy which is converted into heat within the fluid, leading to a rise in fluid temperature. The impact of Soret number S_r on fluid temperature is showcased in Fig. 17. It is clearly seen that fluid temperature is enhanced with larger values of S_r. Physically, mounting values of S_r intensify the thermal energy within the fluid, hence fluid temperature rises. The variation of nanoparticle volume fraction with fluid temperature is exhibited in Fig. 18. It is clearly observed that increasing nanoparticle volume fraction ϕ enhances fluid temperature. This is due to the improvement of thermal conductivity within the fluid regime. The variation of time with respect to fluid temperature is observed in Fig. 19. It is noted that fluid temperature increases as time increases.

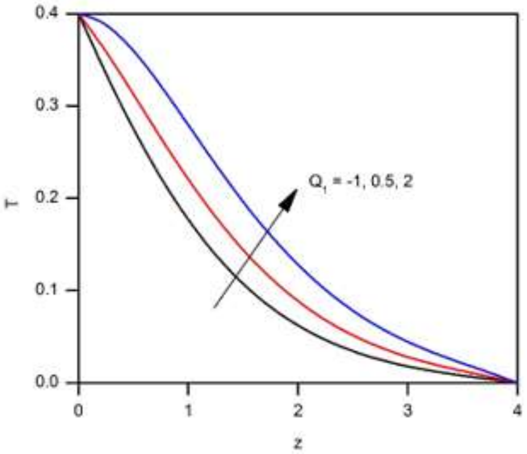

Fig 14: Fluid temperature T with Q_1 values

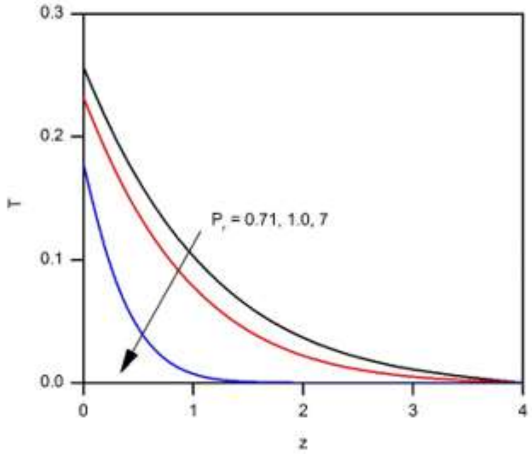

Fig 15: Fluid temperature T with P_r values

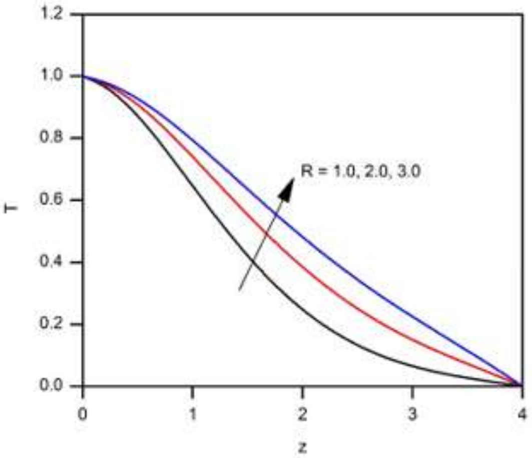

Fig 16: Fluid temperature T with R values

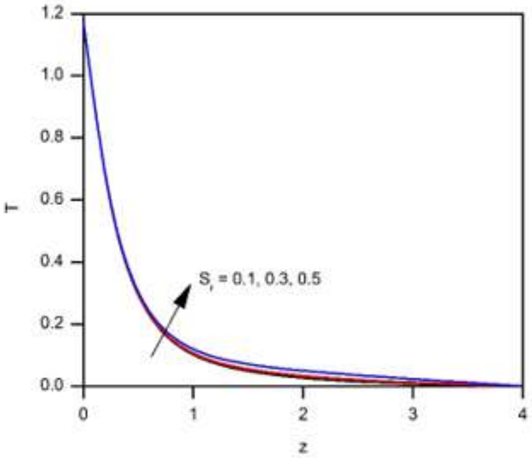

Fig 17: Fluid temperature T with S_r values

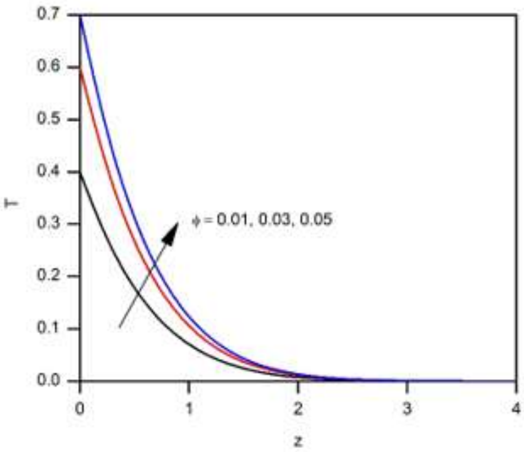

Fig 18: Fluid temperature T with ϕ values

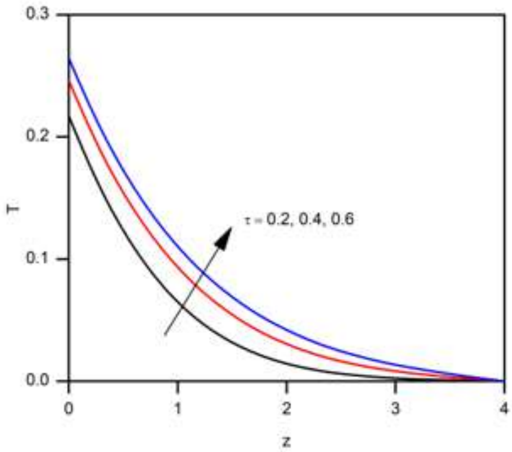

Fig 19: Fluid temperature T with τ values

Concentration profile

Fig 20 illustrates the influence of Schmidt number S_c on the species concentration. Physically, the upsurge of Schmidt number S_c conveys the diminution of molecular diffusion. Consequently, the concentration of the species within the fluid advances for slighter values of S_c and declines for larger values of S_c. The effect of the chemical reaction parameter γ on fluid concentration profile is shown in Fig. 21. It is clearly observed that an increase in the chemical reaction parameter γ drops the species concentration of the fluid. Chemical reaction lowers the movement of the molecules of the fluid, hence lessening the fluid concentration. Fig 22 confirms the variation of fluid concentration species with time τ. It is clearly observed that concentration increases progressively with time τ.

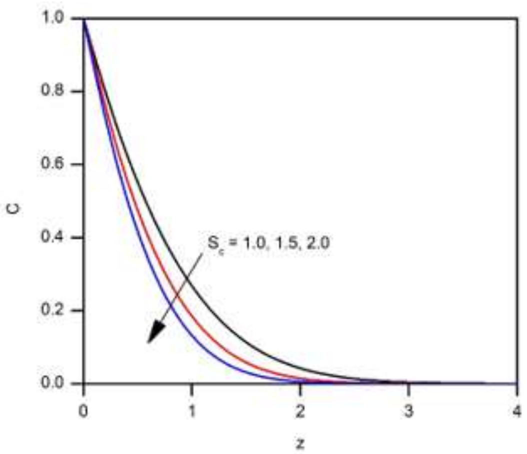

Fig 19: Fig: Species concentration C with S_c values

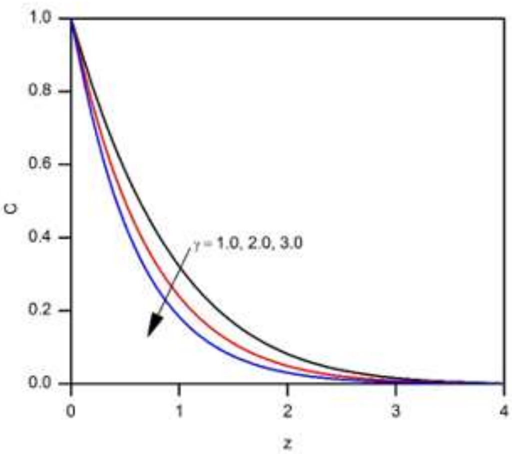

Fig 20: Species concentration C with γ values

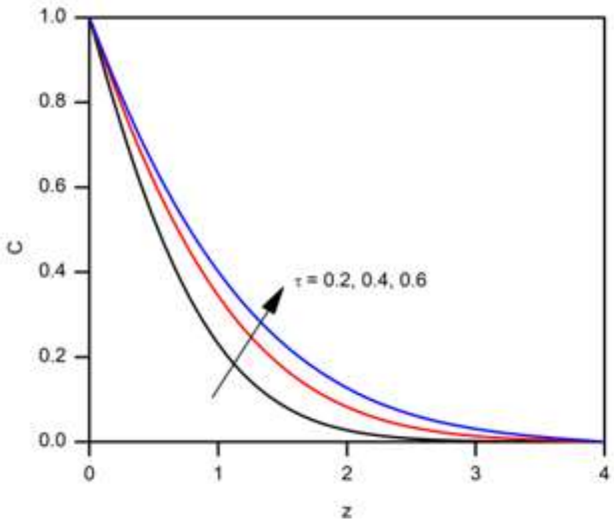

Fig 21: Species concentration C with τ values

Table 2 shows that the Nusselt number increases with rising values of the radiation parameter, porosity parameter, and nanoparticle volume fraction, while an opposing effect is observed with increasing magnetic parameter values. Table 3 shows that skin friction at the plate surface decreases with increasing values of the permeability parameter, heat generation parameter, Soret number, time, thermal Grashof number, and mass Grashof number, while the reverse trend is observed with increasing values of the magnetic parameter, inclination angle, Prandtl number, and radiation parameter. It is clearly seen from Table 4 that increasing values of the chemical reaction parameter and Schmidt number enhance the rate of mass transfer, while increasing the thermo-diffusion parameter reduces the Sherwood number.

Table 3: Alteration of skin friction coefficient for various parameters

G_T	G_C	M	K_1	α	P_r	R	Q_1	C_f
3.00	5.00	4.00	0.70	$\pi/6$	0.71	5.00	2.00	1.335298
5.00								1.071307
	7.00							0.964342
		3.00						0.756555
			1.50					1.099243
				$\pi/3$				1.514562
					0.50			1.285606
						7.00		1.135684
							5.00	1.296732
							1.00	1.022541

Table 4: Variation of the Sherwood number

S_c	S_r	γ	τ	S_h
0.60	2.00	0.10	0.60	0.314773
3.00				1.386539
	3.00			-0.156531
		1.50		0.884287
			0.80	0.934265

CONCLUSIONS

In this work, the governing system of PDEs was solved numerically using a Fortran-based explicit finite difference code, and the results were visualised using Origin 8.5 software, to investigate the effects of thermo-diffusion (Soret) and diffusion-thermo (Dufour) on unsteady MHD free convective nanofluid transport past an inclined vertical porous plate. The principal findings of this study are summarised as follows:

- The velocity and temperature increase with rising values of R_r, Q_1 and τ while an increase in P_r have reverse tendency.
- An upsurge in S_c and γ yields to velocity and concentration decline while reverse effect is noticed when τ progresses.
- Increasing K_1, D_u, G_T and G_C escalates the velocity while increasing M and α have conflicting effect.
- Shear stress decreases with growing values of $G_C, G_T, Q_1, S_r,$ and K_1 while it raises with increasing values of $M, \alpha_c, P_r,$ and R.
- Heat transfer within the fluid upsurges with rise of K_1, ϕ, R while degrades with growing values of M.
- Increasing $S_c, \tau,$ and γ enhances Sherwood number while it lessens with progression of S_r.

The principal novelty of this study lies in the simultaneous treatment of coupled Soret and Dufour effects, thermal radiation, chemical reaction, and heat generation for an unsteady MHD Cu–Ag hybrid nanofluid over an inclined porous plate — a combination not previously addressed in the literature. The results demonstrate that the inclination angle plays a critical role in momentum suppression and can be exploited as a passive flow control parameter in industrial systems such as inclined solar thermal collectors, slanted-wall chemical reactors, and pharmaceutical drying equipment. Quantitatively, increasing the inclination angle from 15° to 75° produces a significant reduction in skin friction, suggesting that oblique configurations offer reduced drag penalties relative to vertical arrangements under comparable flow conditions. Furthermore, the strong sensitivity of the Sherwood number to the Soret parameter indicates that thermo-diffusion effects must be accounted for in the design of mass transfer devices operating under thermal gradients, such as membrane separation units and isotope purification columns.

Future investigations may extend this work by considering non-Newtonian base fluids, variable thermal conductivity, or non-uniform magnetic field distributions, and experimental validation using a Hartmann flow channel would further confirm the practical applicability of the findings reported here.

REFERENCES

S. U. S. Choi, 1995. Enhancing thermal conductivity of fluids with nanoparticles, in developments and applications of non-Newtonian flows, D. A. Siginer, and H. P. Wang, eds., ASME, FED-231/MD- 66, 99-105.

Lee S, Choi SUS, Li S, Eastman JA., 1999. Measuring Thermal Conductivity of Fluids Containing Oxide Nanoparticles. ASME Journal of Heat Transfer. 121(2):280–288.

Hong KS, Hong T-K, Yang H-S., 2006. Thermal conductivity of Fe nanofluids depending on the cluster size of nanoparticles. Applied Physics Letters. 88(3):1–3.

Mustafa M., Khan J. A., Hayat T., Alsedi A., 2015. Boundary layer flow of nanofluid over a nonlinearly stretching sheet with convective boundary condition. IEEE Transactions on nanotechnology. 14 (1), 159–168.

H. Azmi, K. Abdul Hamid, R. Mamat, K.V. Sharma, 2016 Effects of working temperature on thermo-physical properties and forced convection heat transfer of TiO2, nanofluids in water ethylene glycol mixture, Appl. Therm. Eng. 106 (2016) 1190-1199.

Khan W. A., Pop I. Boundary layer flow of a nanofluid past a stretching sheet. International Journal of Heat and Mass Transfer. 53 (11–12), 2477–2483, 2010.

B. Mahanthesh, B. J. Gireesha, R. S. R. Gorla, F. M. Abbasi, and S. A. Shehzad, 2016. “Numerical solutions for magnetohydrodynamic flow of nanofluid over a bidirectional non-linear stretching surface with prescribed surface heat flux boundary,” Journal of Magnetism and Magnetic Materials, vol. 417, pp. 189–196.

T. Hayat, S. Nadeem, 2017. Heat transfer enhancement with Ag–CuO/water hybrid nanofluid, Results Phys 7 2317–2324.

L.S. Sundar, K.V. Sharma, M.K. Singh, A.C.M. Sousa, Hybrid nanofluids preparation, thermal properties, heat transfer and friction factor – a review, Renew. Sustain. Energy Rev. 68, 185–198

Balla, C. S., Alluguvelli, R., Naikoti, K., and Makinde, O. D., 2020. Effect of chemical reaction on bioconvective flow in oxytactic microorganisms suspended porous cavity. Journal of Applied and Computational Mechanics, 6(3), 653-664.

Shamshuddin, M. D., Abderrahmane, A., Koulali, A., Eid, M. R., Shahzad, F., and Jamshed, W., 2021. Thermal and solutal performance of Cu/CuO nanoparticles on a non-linear radially stretching surface with heat source/sink and varying chemical reaction effects. International Communications in Heat and Mass Transfer, 129, 105710.

Puneeth, V., Manjunatha, S., Makinde, O. D., and Gireesha, B. J., 2021. Bioconvection of a radiating hybrid nanofluid past a thin needle in the presence of heterogeneous–homogeneous chemical reaction. Journal of Heat Transfer, 143(4), 042502.

Arshad, M., Hussain, A., Hassan, A., Haider, Q., Ibrahim, A. H., Alqurashi, M. S., ... and Abdussattar, A., 2021. Thermophoresis and brownian effect for chemically reacting magneto-hydrodynamic nanofluid flow across an exponentially stretching sheet. Energies, 15(1), 143.

Biswas, R., Hossain, M. S., Islam, R., Ahmmed, S. F., Mishra, S. R., and Afikuzzaman, M., 2022. Computational treatment of MHD Maxwell nanofluid flow across a stretching sheet considering higher-order chemical reaction and thermal radiation. Journal of Computational Mathematics and Data Science, 4, 100048.

Shamshuddin, M. D., Shahzad, F., Jamshed, W., Bég, O. A., Eid, M. R., and Bég, T. A., 2023. Thermo-solutal stratification and chemical reaction effects on radiative magnetized nanofluid flow along an exponentially stretching sensor plate: Computational analysis. Journal of Magnetism and Magnetic Materials, 565, 170286.

Reddy, Y. D., Goud, B. S., Chamkha, A. J., and Kumar, M. A., 2022. Influence of radiation and viscous dissipation on MHD heat transfer Casson nanofluid flow along a nonlinear stretching surface with chemical reaction. Heat Transfer, 51(4), 3495-3511.

Roja, A., and Gireesha, B. J., 2020. Impact of Hall and Ion effects on MHD couple stress nanofluid flow through an inclined channel subjected to convective, hydraulic slip, heat generation, and thermal radiation. Heat Transfer, 49(6), 3314-3333.

Kumar, M. A., Reddy, Y. D., Rao, V. S., and Goud, B. S., 2021. Thermal radiation impact on MHD heat transfer natural convective nanofluid flow over an impulsively started vertical plate. Case studies in thermal engineering, 24, 100826.

Suresh Kumar, Y., Hussain, S., Raghunath, K., Ali, F., Guedri, K., Eldin, S. M., and Khan, M. I., 2023. Numerical analysis of magnetohydrodynamics Casson nanofluid flow with activation energy, Hall current and thermal radiation. Scientific Reports, 13(1), 4021.

Makinde, O. D., and Aziz, A., 2011. Boundary layer flow of a nanofluid past a stretching sheet with a convective boundary condition. International Journal of Thermal Sciences, 50(7), 1326-1332.

Shamshuddin, M. D., Akkurt, N., Saeed, A., and Kumam, P., 2023. Radiation mechanism on dissipative ternary hybrid nanoliquid flow through rotating disk encountered by Hall currents: HAM solution. Alexandria Engineering Journal, 65, 543-559.

Salawu, S. O., Obalalu, A. M., Fatunmbi, E. O., and Shamshuddin, M. D., 2023. Elastic deformation of thermal radiative and convective hybrid SWCNT-Ag and MWCNT-MoS4 magneto-nanofluids flow in a cylinder. Results in Materials, 17, 100380.

Reddy, Y. D., Goud, B. S., 2023. Comprehensive analysis of thermal radiation impact on an unsteady MHD nanofluid flow across an infinite vertical flat plate with ramped temperature with heat consumption. Results in Engineering, 17, 100796.

Gopal H.K, Sundhakar M, and Masthan Rao S., 2023. Unsteady Magnetohydrodynamics (MHD) natural convective flow of nanfluids over an infinite perpendicular absorbent plate. J. of nanofluids Vol.12, pp. 280-287.

Singha, A. K., Seth, G. S., Bhattacharyya, K., Yadav, D., Verma, A. K., and Gautam, A. K., 2021. Soret and Dufour effects on hydromagnetic flow of H2O-based nanofluids induced by an exponentially expanding sheet saturated in a non-Darcian porous medium. Journal of Nanofluids, 10(4), 506-517.

Padmaja, K., and Rushi Kumar, B., 2022. Dufour and Soret Effects on MHD Flow of Cu-Water and Al 2 O 3-Water Nanofluid Flow Over a Permeable Rotating Cone. In Fuzzy Mathematical Analysis and Advances in Computational Mathematics (pp. 221-236). Singapore: Springer Singapore.

Siddique, I., Nadeem, M., Awrejcewicz, J., and Pawłowski, W., 2022. Soret and Dufour effects on unsteady MHD second-grade nanofluid flow across an exponentially stretching surface. Scientific Reports, 12(1), 11811.

Haritha, A., Vishali, B., and Venkata Lakshmi, C., 2023. Heat and mass transfer of MHD Jeffrey nanofluid flow through a porous media past an inclined plate with chemical reaction, radiation, and Soret effects. Heat Transfer, 52(2), 1178-1197.

Raghunath, K., 2023. Study of Heat and Mass Transfer of an Unsteady Magnetohydrodynamic (MHD) Nanofluid Flow Past a Vertical Porous Plate in the Presence of Chemical Reaction, Radiation and Soret Effects. Journal of Nanofluids, 12(3), 767-776.